Journal of Power Sources 195 (2010) 313–319

Contents lists available at ScienceDirect

Journal of Power Sources

journal homepage: www.elsevier.com/locate/jpowsour

Self-assembled synthesis of hierarchical nanostructured CuO with various morphologies and their application as anodes for lithium ion batteries

J.Y. Xiang, J.P. Tu*, L. Zhang, Y. Zhou, X.L. Wang, S.J. Shi

State Key Laboratory of Silicon Materials and Department of Materials Science and Engineering, Zhejiang University, Zheda Road, No. 38, Hangzhou 310027, China

ARTICLE INFO

Article history:
Received 25 June 2009
Received in revised form 10 July 2009
Accepted 13 July 2009
Available online 21 July 2009

Keywords:
Copper oxide
Morphology
Self-assembled
Anode
Lithium ion battery

ABSTRACT

We report a simple self-assembled synthesis of hierarchical CuO particles with various morphologies such as leaf, shuttle, flower, dandelion, and caddice clew. The morphologies can be easily tailored by adjusting the pH value. The synthesis is based on dehydration and re-crystallization of precursor $Cu(OH)_2$ nanowires. $[Cu(NH_3)_4]^{2+}$ and OH^- in the solutions are considered as the key factors to influence the assembling manner of CuO. The obtained hierarchical CuO particles serve as a good model system for the study as anodes for lithium ion batteries. Various morphologies of CuO particles result in different electrochemical performances of electrodes. Compared to others, dandelion-like and caddice clew-like CuO exhibit reversible discharge capacities of 385 mAh g^{-1} and 400 mAh g^{-1} at 0.1 C, 340 mAh g^{-1} and 374 mAh g^{-1} at 0.5 C after 50 cycles, respectively. The higher discharge capacities and better cycling performances are attributed to their larger surface area and porosity, leading to better contact between CuO and electrolyte and shorter diffusion length of lithium ions.

1. Introduction

Recently, 3d transition metal oxides (MO, where M is Fe, Co, Ni, and Cu) have been widely investigated as promising anodes for lithium ion batteries since they were firstly proposed by Tarascon et al. [1]. Comparing to the current commercial carbonaceous anodes, 3d transition oxides have much higher theoretic capacity and better rate property, which will hopefully realize the wide application of Li ion batteries in various fields such as electric vehicles, military, and the like [2–5]. Among these transition metal oxides, CuO has been paid more attentions due to its attractive advantages as high theoretic capacity (670 mAh g^{-1}), inexpensive, non-toxic, easily produced, and readily stored. For the past several years, various structured CuO with different sizes, such as hollow dandelion-like spheres, nanoflower, nanorod, and nanotube, have been synthesized as anodes for lithium ion batteries, which exhibit much different electrochemical performances [6–10]. Thus, the morphology and microstructure of CuO anode may be taken into careful consideration since the contact between active material and electrolyte, diffusion length for Li^+, and area of SEI film, which influence the electrochemical properties, are tightly related to its morphology. Although some approaches have been developed to study the formation mechanism of CuO with various morphologies [11–13], not many investigations have been done on the morphology effect on the electrochemical properties of CuO as anode for lithium ion batteries. Hence, in this present work, we developed a simple self-assembled synthesis of hierarchical CuO particles with various morphologies such as leaf, shuttle, flower, dandelion, and caddice clew. The morphology transformation mechanism is discussed and their electrochemical performances are investigated.

2. Experimental

The self-assemble of CuO particles with various morphologies was carried out according to the following procedures. Different amount of ammonia was added to the aqueous solution of $Cu(Ac)_2{\cdot}H_2O$ (0.01 M) and adjust the pH value of the solutions to 9.5, 10, 10.5, 11, 11.5 and 12, respectively. Several minutes later, flocky precipitates appeared in these blue solutions except for the solution with pH 12. And then the solutions were heated and kept in Petri dishes at 90 °C for 12 h. The colors of the solutions became light and even colorless, and black precipitates were obtained at the bottom of the dishes. Finally, the precipitates were separated by centrifugation, washed with deionized water and ethanol for several times, and dried in vacuum at 60 °C for 24 h.

The structure and morphology of the as-prepared particles were analyzed by X-ray diffraction (XRD, Philips PC-APD with Cu Kα radiation), field emission scanning electron microscopy (FESEM, FEI SIRION) and high-resolution transmission electron microscopy (HRTEM, JEOL JEM-2010F), respectively.

Electrochemical performances of the CuO particles with different morphologies were investigated with two-electrode coin-type

* Corresponding author. Tel.: +86 571 8795 2573; fax: +86 571 8795 2856.
E-mail address: tujp@zju.edu.cn (J.P. Tu).

0378-7753/$ – see front matter © 2009 Elsevier B.V. All rights reserved.
doi:10.1016/j.jpowsour.2009.07.022

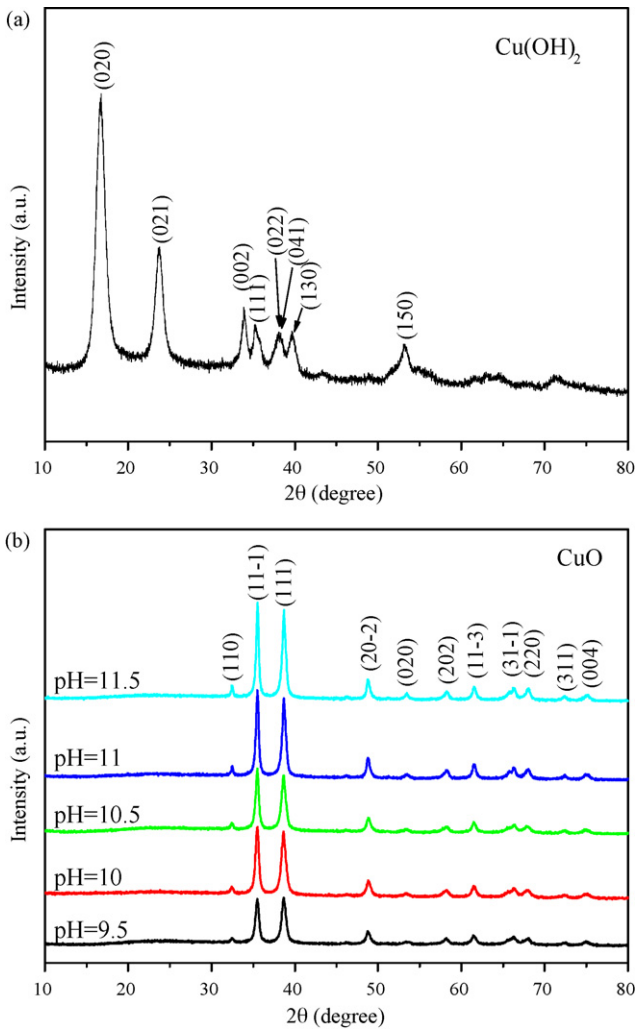

Fig. 1. XRD patterns of (a) $Cu(OH)_2$ precursor precipitated at room temperature and (b) CuO particles obtained after the solutions are heated at 90 °C for 12 h.

cells (CR 2025). The working electrodes were prepared by a slurry coating procedure. The slurry consisted of 80 wt.% CuO particles, 10 wt.% acetylene black and 10 wt.% polyvinylidene fluoride (PVDF) dissolved in N-methyl pyrrolidinone (NMP), and was incorporated on nickel foam with 12 mm in diameter. After dried at 90 °C for 24 h in vacuum, the foam was pressed under a pressure of 20 MPa. The loading density of CuO obtained under different pH conditions varies from 9.5 to 11.5 is 8.85 mg cm^{-2}, 12.28 mg cm^{-2}, 10.62 mg cm^{-2}, 9.46 mg cm^{-2} and 8.57 mg cm^{-2}, respectively. Test cells were assembled in an argon-filled glove box with the metallic lithium foil as both the reference and counter electrodes, 1 M $LiPF_6$ in ethylene carbonate (EC)–dimethyl carbonate (DME) (1:1 in volume) as the electrolyte, and a polypropylene (PP) micro-porous film (Cellgard 2300) as the separator.

The galvanostatic charge–discharge tests were conducted on LAND battery program-control test system at rates of 0.1 C and 0.5 C (1 C = 670 mA g^{-1}) in the voltage range of 0.02–3.0 V (versus Li/Li^+) at room temperature (25 ± 1 °C). Cyclic voltammetry (CV) was performed on CHI660C electrochemical workstation at a scan rate of 0.1 mV s^{-1} from 0 V to 3.0 V.

3. Results and discussion

The precursors precipitated in the solutions with pH values vary from 9.5 to 11.5 at room temperature have the similar XRD patterns as shown in Fig. 1a. All the diffraction peaks correspond well with orthorhombic $Cu(OH)_2$ (space group *Cmcm*(63), JCPDS 35-0505). Broadening in the peaks of $Cu(OH)_2$ indicates the formation of $Cu(OH)_2$ nanostructures. Fig. 1b shows the XRD patterns of the samples after the solutions are held at 90 °C for 12 h. All the diffraction peaks of these samples can be perfectly indexed to monoclinic CuO (space group *C*2/*c*, JCPDS 48-1548) with lattice constants $a = 4.688$ Å, $b = 3.423$ Å, $c = 5.132$ Å. The reactions for CuO precipitation can be summarized as follows:

$$Cu^{2+} + 2NH_3{\cdot}H_2O \rightarrow Cu(OH)_2\downarrow + 2NH_4{}^+ \quad (1)$$

$$Cu(OH)_2 \xrightarrow{90\ ^\circ C} CuO + H_2O \quad (2)$$

CuO precipitates are obtained after the solution containing $Cu(OH)_2$ precursors is heated at 90 °C for 12 h. However, $Cu(OH)_2$ can be dissolved due to the complexing reaction for the existence of excess $NH_4{}^+$ and free NH_3 in the solution. The reaction is simply illustrated as below:

$$Cu(OH)_2 + 4NH_3 + 2NH_4{}^+ \rightarrow [Cu(NH_3)_4]^{2+} + 2NH_3{\cdot}H_2O \quad (3)$$

Obviously, the concentration of ammonia will affect the solubility of $Cu(OH)_2$. And the competition balance between reaction (2) and (3) is the key factor to successfully prepare CuO. If the ammonia concentration is too high, the fresh $Cu(OH)_2$ precipitation will react with large numbers of excess $NH_4{}^+$ and NH_3 and be dissolved immediately. This is the reason why there is no precipitation occurs in the solution with pH 12. Similar phenomenon of nano-NiO preparation via ammonia precipitation has been discussed by Xiang and Zhong [14]. In addition, different pH values will no doubt lead to differ-

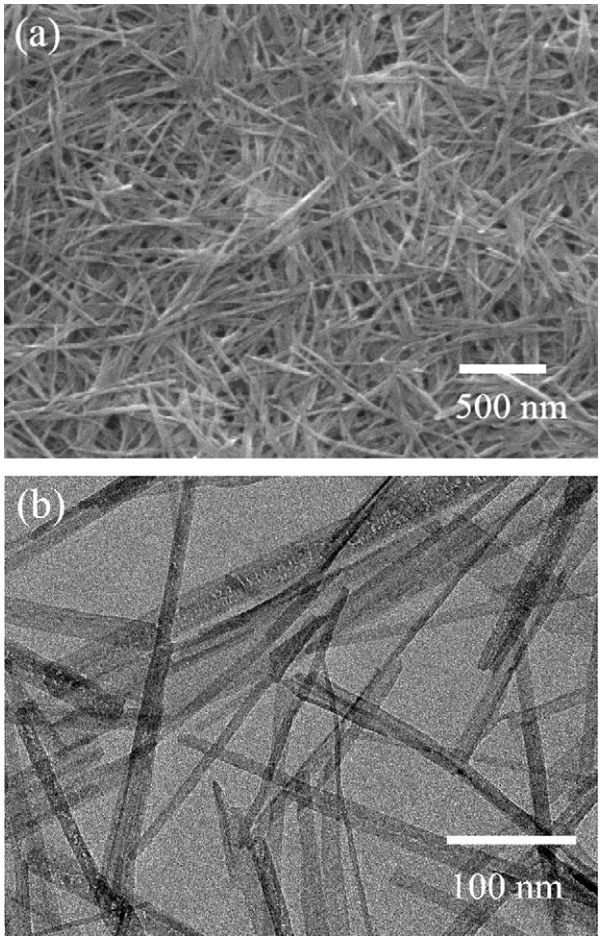

Fig. 2. (a) SEM image and (b) TEM image of $Cu(OH)_2$ precursor.

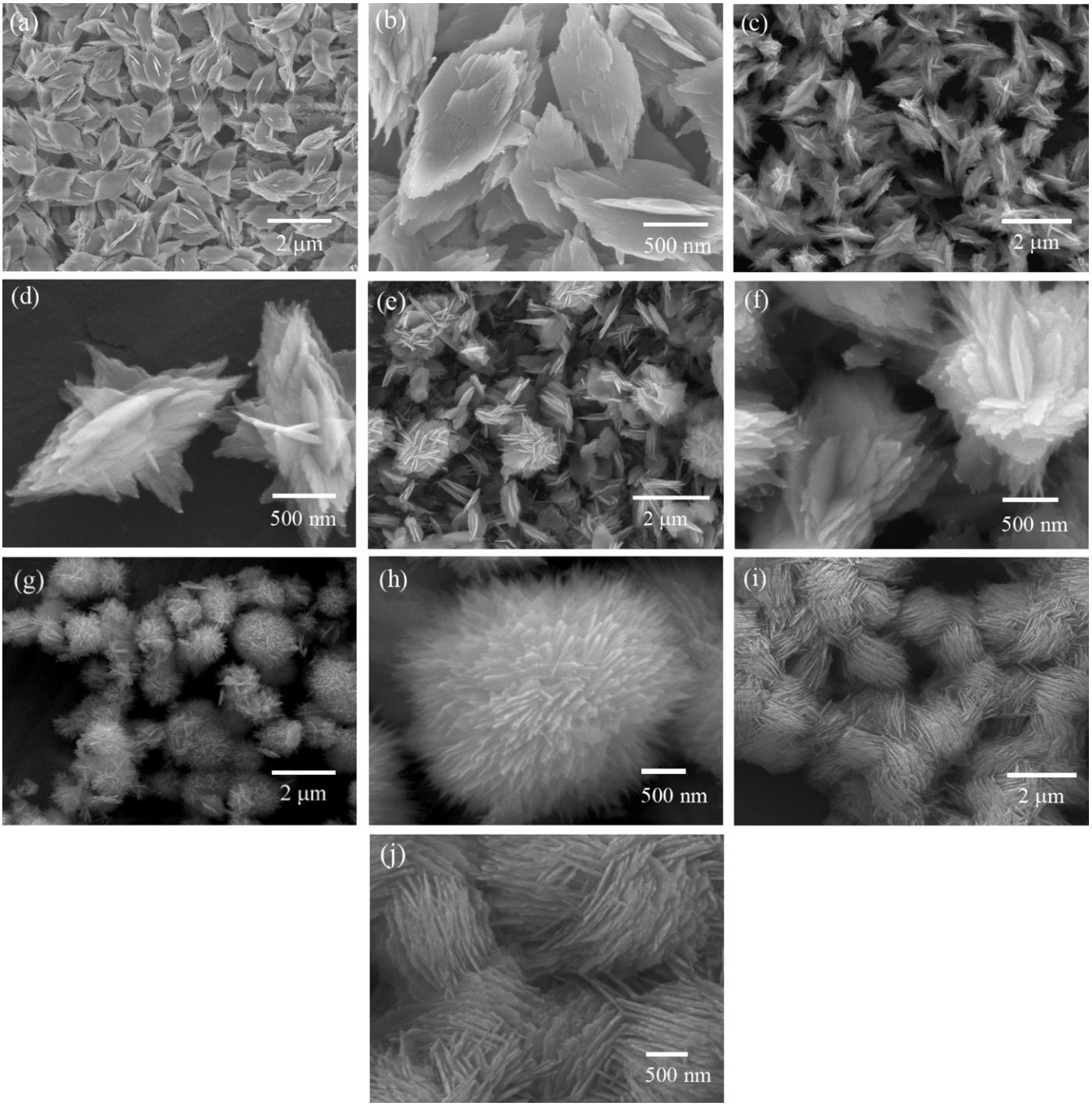

Fig. 3. SEM images of CuO particles obtained under different pH conditions: (a), (b) pH 9.5; (c), (d) pH 10; (e), (f) pH 10.5; (g), (h) pH 11 and (i), (j) pH 11.5.

ent concentrations of $[Cu(NH_3)_4]^{2+}$ and OH^- in the solutions, and finally result in the formation of CuO with various morphologies.

Fig. 2 shows the SEM and TEM images of $Cu(OH)_2$ precursor precipitated from ammonia solution. It is noticed that $Cu(OH)_2$ precursor exhibits a highly dispersed nanowire morphology. The nanowires are 5–10 nm in diameters and 300–400 nm in lengths. This kind of nanowires can be formed in all the solutions with pH values from 9.5 to 11.5. The morphologies of CuO particles dehydrated from $Cu(OH)_2$ are shown in Fig. 3. Various shapes of CuO are obtained by changing the pH value of the solutions. The CuO particles synthesized in the solution with pH 9.5 show a leaf-shaped morphology (Fig. 2a). The CuO leaves are about 1 μm in length, 500 nm in width and 100–200 nm in thickness. As the pH value increases, the morphology of the particles becomes more and more three-dimensional. The CuO particles prepared in the solution with pH 10 are shuttle-shaped with the entire surface covered with branches (Fig. 2b). When pH 10.5, the as-prepared CuO is flower-like and composed of several 2D nanosheets, which are about 500 nm in width and 50–100 nm in thickness (Fig. 2c). As the pH value increases to 11, the CuO particles look like dandelions and exhibit a hierarchical system, in which the skeleton is made up of sphere with diameters of 2–4 μm possessing a large number of 2D feathers (Fig. 2d). The nanofeathers are less than 50 nm in thickness, thinner than the flower petals in Fig. 2c. When pH 11.5, caddice clew-like

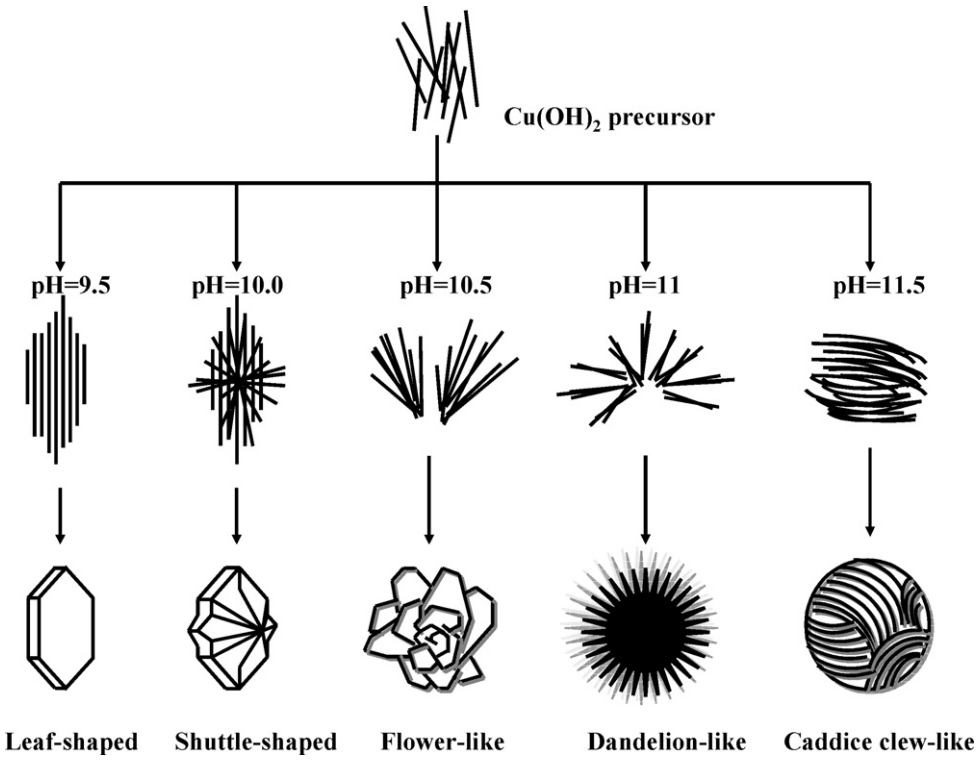

Fig. 4. Schematic illustration of the growth of CuO particles under different pH conditions.

CuO spheres are obtained. The hierarchical spheres are convoluted by thousands of nanowires, which are about 20 nm in diameter and 1 μm in length (Fig. 2e). The size of the caddice clew-like sphere is also about 2–4 μm.

The notable difference on morphology of CuO has great relationship with the pH value of the solution. Schematic illustration of the transformation from $Cu(OH)_2$ to CuO is presented in Fig. 4. $Cu(OH)_2$ nanowires are formed in all the mixed solution of $NH_3{\cdot}H_2O$ and $Cu(Ac)_2{\cdot}H_2O$ with pH values from 9.5 to 11.5. However, after heating these solutions at 90 °C for 12 h, $Cu(OH)_2$ is changed into CuO and the morphologies of CuO precipitates change a lot. In the solution with pH 9.5, $Cu(OH)_2$ nanowires assemble closely parallel to their length and become leaf-shaped particles after dehydration. As the pH value increases to 10, $Cu(OH)_2$ nanowires assemble not only parallel, but also vertical to their length, thus shuttle-shaped particles are formed. When pH 10.5, 2D nanosheets are firstly assembled, and then CuO flowers are grown up with the nanosheets as flower petals. In the solution with pH 11, a great many of thin feathers are formed instead of 2D nanosheets by the gather of $Cu(OH)_2$ nanowires. The clusters of nanofeathers finally become dandelion-like spheres. When pH 11.5, $Cu(OH)_2$ nanowires convolute together and become caddice clew-like spheres rather than thin feathers. Obviously, with increasing the pH value, the $Cu(OH)_2$ nanowires behave more and more active, and prefer to form more three-dimensional and hierarchical nanostructured CuO. It can be attributed to the competition balance between dehydration and dissolving of $Cu(OH)_2$. As presented in Eqs. (2) and (3), the concentration of $[Cu(NH_3)_4]^{2-}$ increases with the pH value. Ammonia complexing cations are known as activation catalyst and can enhance the reaction kinetics [15,16]. Hence, it is considered that the existence of $[Cu(NH_3)_4]^{2+}$ in the solution results in the faster or slower reaction kinetics, which is responsible for the different assembling manners of $Cu(OH)_2$. In addition, the concentration of OH^- is supposed to have a significant effect on the nucleation and growth (such as the number of nuclei and the concentration of growth units) behavior of CuO nanocrystals [12]. This is also the reason for the various morphologies of CuO precipitated under different pH conditions.

Fig. 5 displays the first three discharge–charge curves for CuO with different morphologies between 0.02 V and 3.0 V at 0.1 C. All the electrodes exhibit similar discharge behavior. Three plateaus at the potential of 1.6–1.8 V, 1.1–0.3 V and 0.7–0.9 V appear in the first discharge curves, and corresponds to the reductive reaction from CuO to intermediate composite copper oxide phase, to Cu_2O and further decomposition into Cu and Li_2O, respectively [17]. In the first charge curves, only two inclined plateaus near 2.5 V and 1.5 V can be observed, and are corresponding to the process $2Cu + Li_2O \rightarrow Cu_2O + 2Li$ and the partial oxidation of Cu_2O to CuO, respectively. However, the first discharge capacities and initial coulombic efficiencies of these electrodes are different from each other. The samples obtained in the solutions with pH values from 9.5 to 11.5 exhibit first discharge capacity as 740 mAh g^{-1}, 773 mAh g^{-1}, 847 mAh g^{-1}, 927 mAh g^{-1} and 952 mAh g^{-1}, and initial coulombic efficiency as 69.1%, 69.5%, 71.1%, 62.1% and 62.5%, respectively. These differences in capacity and coulombic efficiency can be attributed to the different morphology of CuO electrodes. The leaf-shaped and shuttle-shaped CuO precipitated at pH 9.5 and 10 are solid and about 1 μm in size. Only the surface of the leaf and shuttle can be contacted with electrolyte, and result in fewer sites to accommodate Li^+. Hence, the first discharge capacities of the leaf-shaped and shuttle-shaped CuO are lower than those of other electrodes. As the pH value increases, the morphology of CuO transfers to flower-like, dandelion-like, and caddice clew-like. Although the size of CuO increases a little with the rise of pH value, the specific surface of each particle is not decreasing, but even become larger for its hierarchical nanostructured morphology. The larger specific surface of nanosheets, nanofeathers and nanowires provide more contact area between CuO and electrolyte and offers more sites to accommodate Li^+, leading to higher initial discharge capacity. The caddice clew-like CuO sphere convoluted of thousands of nanowires (about 20 nm in diameter)

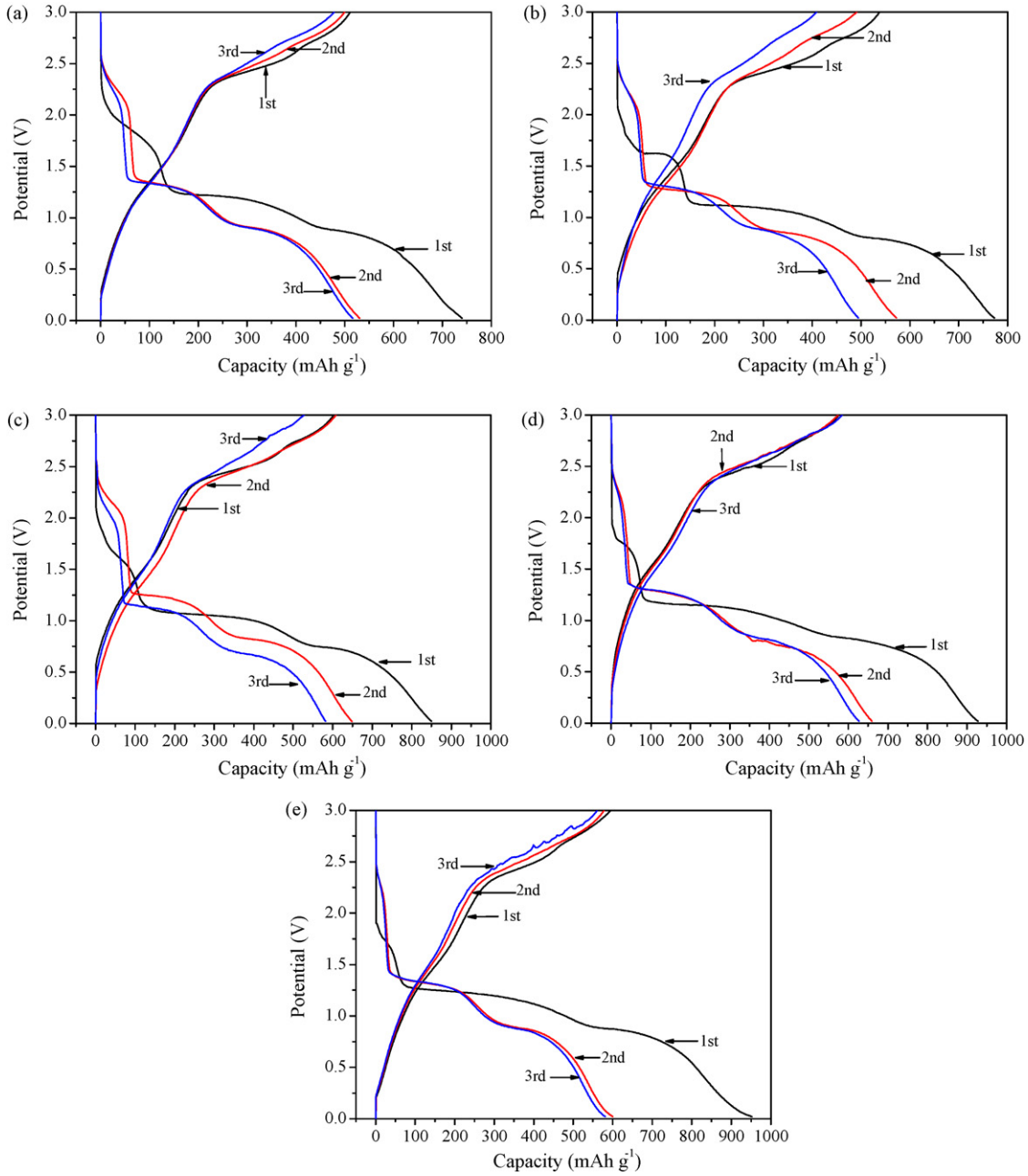

Fig. 5. The discharge–charge curves for CuO particles under different pH conditions: (a) pH 9.5, (b) pH 10, (c) pH 10.5, (d) pH 11 and (e) pH 11.5.

exhibit the highest first discharge capacity among the five electrodes.

However, the initial coulombic efficiency of CuO electrodes does not grow up with increasing the pH value. As shown in Fig. 6, CuO particles obtained in the solutions with pH values from 9.5 to 10.5 show relatively high initial coulombic efficiencies (about 68–71%), while the ones precipitated in the solutions with pH 11 and 11.5 exhibit lower initial coulombic efficiencies (about 62%). It can be explained that fully contact between CuO and electrolyte not only offers more site for Li^+ accommodation, but also increases the area for SEI film during the first discharging process. SEI film is known as a gel-like layer which contains ethylene oxide based oligomers, LiF, Li_2CO_3, and lithium alkyl carbonate ($ROCO_2Li$) [18]. The incompletely decomposition of SEI is the main reason for the low coulombic efficiency and large capacity loss during the initial cycle, which happens in all 3d transition metal oxides including CuO, NiO, Co_3O_4 [19–23]. For the dandelion-like and caddice clew-like CuO, a great deal of SEI film is formed on the surface of hierarchical nanostructure. The large area of SEI film can not be decomposed sufficiently in the first charging process, thus leads to the lower initial coulombic efficiency of the CuO electrodes. Therefore, under the two-faced effect of specific surface, the flower-like CuO precipitated at pH 10.5 shows the best electrochemical performances during the first cycle, exhibiting the discharge capacity of 847 mAh g^{-1} and coulombic efficiency of 71%, as presented in Fig. 6.

Fig. 7 shows the cycling performance of CuO with different morphologies. The dandelion-like and caddice clew-like CuO show higher reversible capacities and much better capacity retention than those of leaf-shaped and shuttle-shaped CuO. The reversible capacity of hierarchical CuO spheres precipitated at pH 11.5 is 400 mAh g^{-1} at 0.1 C, and 375 mAh g^{-1} at 0.5 C. For the leaf-shaped CuO obtained in the solution with pH 9.5, the reversible capac-

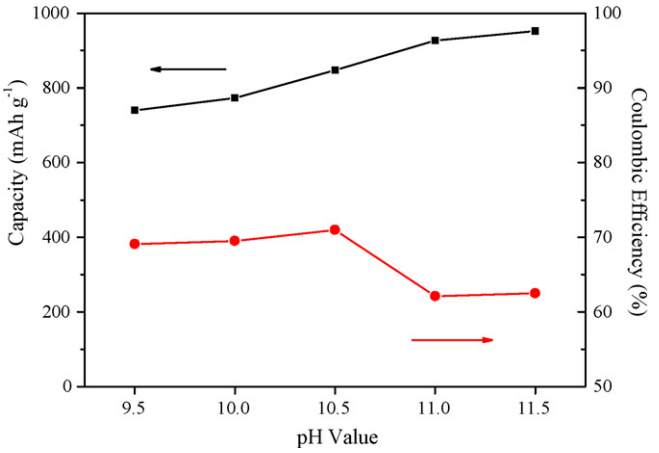

Fig. 6. The initial discharge capacities and coulombic efficiencies of CuO electrodes.

ity is only 300 mAh g^{-1} at 0.1 C, and 180 mAh g^{-1} at 0.5 C. The good capacity retention and rate properties of dandelion-like and caddice clew-like CuO are attributed to their hierarchical nanostructures. The nanofeathers and nanowires, which build up the CuO microspheres, are less than 50 nm in width, which makes the diffusion length of Li^+ is shorter than 25 nm. However, the leaf-shaped and shuttle-shaped CuO can only provide limited contact area with electrolyte and lead to much longer Li^+ diffusion length. Hence, hierarchical nanostructured CuO spheres can react with Li^+ much faster on the surface and inner parts than solid leaf-shaped and shuttle-shaped CuO, even at high current density. In addition, the large specific surface area will reduce the specific current density in hierarchical nanostructured CuO. Therefore, the CuO with dandelion-like and caddice clew-like morphologies can exhibit much better cycling performance than the CuO with other morphologies especially at high current density.

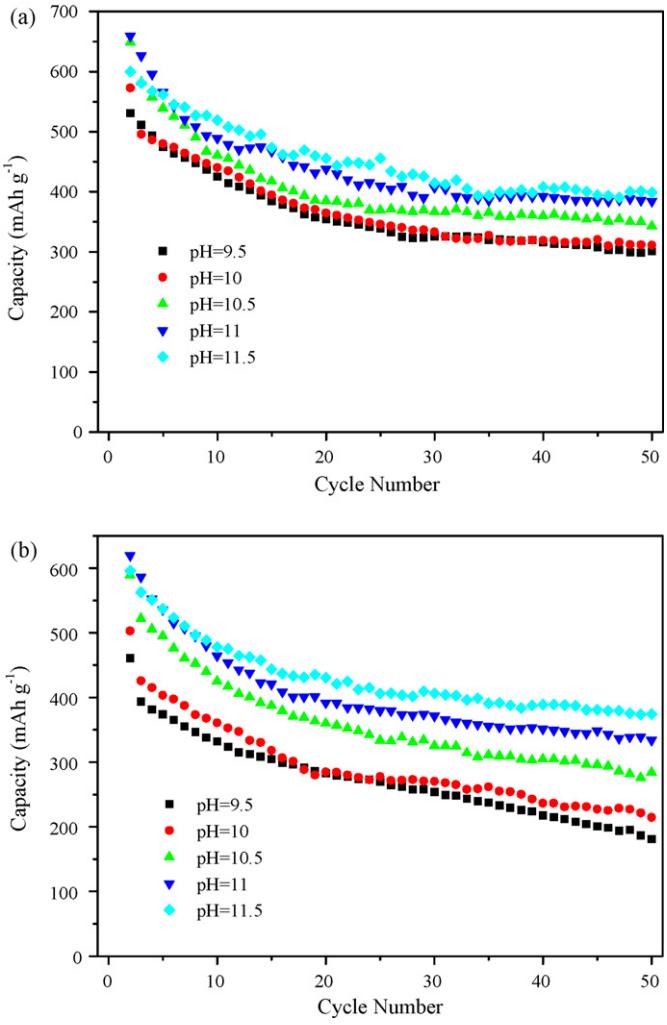

Fig. 7. Cycling performances of CuO electrodes at rates of: (a) 0.1 C and (b) 0.5 C (from the 2nd cycle to the 50th cycle).

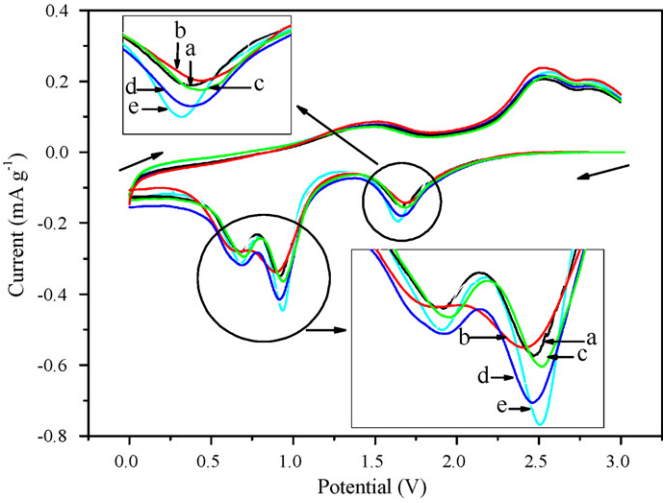

Fig. 8. The first cyclic voltammogram curves for CuO electrodes obtained under different pH conditions: (a) pH 9.5, (b) pH 10, (c) pH 10.5, (d) pH 11, (e) pH 11.5 at a scan rate of 0.1 mV s^{-1} from 0 V to 3.0 V.

The cyclic voltammogram curves are tested to further investigate the electrochemical behaviors of CuO with different morphologies, as shown in Fig. 8. The cathodic and anodic peaks are all corresponding well with the discharge–charge plateaus in Fig. 5. These peaks locating at the potential of 0.7 V, 1.0 V and 1.7 V correspond to the reduction from CuO to intermediate composite copper oxide phase, to Cu_2O and further decomposition into Cu and Li_2O, respectively. The shapes of the CV curves for the five electrodes are similar to each other. Nevertheless, the cathodic peaks of dandelion-like and caddice clew-like CuO are more intensive than those of other CuO electrodes. Large area of these peaks means larger amount of Li^+ react with CuO in the discharging process. So the discharge capacities of dandelion-like and caddice clew-like CuO should be higher than those of other CuO electrodes, which is consistent with the results presented in Fig. 6.

What's more, the differences of areas between cathodic and anodic peaks for these CuO electrodes also differ from each other. The smaller the difference in areas of cathodic and anodic peaks, the higher the coulombic efficiency of the electrode. Hence, it is confirmed that the leaf-shaped, shuttle-shaped and flower-like CuO exhibit higher initial coulombic efficiency than dandelion-like and caddice clew-like CuO by comparing the cathodic and anodic peaks in their CV curves.

4. Conclusions

Different copper oxide particles (leaf-shaped, shuttle-shaped, flower-like, dandelion-like and caddice clew-like) were self-assembled in the mixed solutions of aqueous ammonia and $Cu(Ac)_2{\cdot}H_2O$ with pH values from 9.5 to 11.5. The assembling manner of $Cu(OH)_2$ precursor is mainly influenced by the concentration of $[Cu(NH_3)_4]^{2+}$ and OH^- in the solution. Hierarchical nanostructured CuO, such as dandelion-like and caddice clew-like spheres can

be self-assembled under higher pH conditions. The electrochemical performances of CuO are tightly related to their morphologies. The leaf-shaped and shuttle-shaped CuO exhibit high initial coulombic efficiency but relatively low discharge capacities for their small specific surface, which limits the large formation of inactive SEI film but reduce the accommodation of Li^+ at the same time. For the dandelion-like and caddice clew-like CuO, although the initial coulombic efficiencies are a little lower, the discharge capacities and cycling properties are much better than the leaf-shaped and shuttle-shaped CuO, especially at high rate. It is attributed to the hierarchical nanostructures, which provide high specific surface area, leading to large contact area for CuO/electrolyte and shorter diffusion length of Li^+.

References

[1] P. Poizot, S. Laruelle, S. Grugeon, L. Dupont, J.M. Tarascon, Nature 407 (2000) 496–499.
[2] S. Mitra, P. Poizot, A. Finke, J.M. Tarascon, Adv. Funct. Mater. 16 (2006) 2281–2287.
[3] G.X. Wang, Y. Chen, K. Konstantinov, M. Lindsay, H.K. Liu, S.X. Dou, J. Power Sources 109 (2002) 142–147.
[4] X.H. Huang, J.P. Tu, C.Q. Zhang, J.Y. Xiang, Electrochem. Commun. 9 (2007) 1180–1184.
[5] J. Morales, L. Sanchez, F. Martin, J.R. Ramos-Barrado, M. Sanchez, Electrochim. Acta 49 (2004) 4589–4597.
[6] S.Q. Wang, J.Y. Zhang, C.H. Chen, Scripta Mater. 57 (2007) 337–340.
[7] J.Y. Xiang, J.P. Tu, Y.F. Yuan, X.L. Wang, X.H. Huang, Z.Y. Zeng, Electrochim. Acta 54 (2009) 1160–1165.
[8] X.P. Gao, J.L. Bao, G.L. Pan, H.Y. Zhu, P.X. Huang, F. Wu, D.Y. Song, J. Phys. Chem. B 108 (2004) 5547–5551.
[9] J.Y. Xiang, J.P. Tu, X.H. Huang, Y.Z. Yang, J. Solid State Electrochem. 8 (2008) 941–945.
[10] S. Grugeon, S. Laruelle, R. Herrera-Urbina, L. Dupont, P. Poizot, J.M. Tarascon, J. Electrochem. Soc. 148 (2001) A285–A292.
[11] J.C. Park, J. Kim, H. Kwon, H. Song, Adv. Mater. 21 (2009) 803–807.
[12] D.P. Singh, A.K. Ojha, O.N. Srivastava, J. Phys. Chem. C 113 (2009) 3409–3418.
[13] M.A. Dar, Q. Ahsanulhaq, Y.S. Kim, J.M. Sohn, W.B. Kim, H.S. Shin, Appl. Surf. Sci. 255 (2009) 6279–6284.
[14] Y.D. Xiang, C. Zhong, Mater. Lett. 58 (2004) 267–280.
[15] B. Beena, U. Chudasama, Transit. Met. Chem. 20 (1995) 166–169.
[16] L. Badr, R. Sultan, Chem. Phys. Lett. 20 (2008) 40–44.
[17] A. Debart, L. Dupont, P. Poizot, D. Larcher, J.M. Tarascon, J. Electrochem. Soc. 148 (2001) A1266–A1274.
[18] G. Gachot, S. Grugeon, M. Armand, S. Pilard, P. Guenot, J.M. Tarascon, S. Laruelle, J. Power Sources 178 (2008) 409–421.
[19] J.Y. Xiang, J.P. Tu, Y.F. Yuan, X.H. Huang, Y. Zhou, L. Zhang, Electrochem. Commun. 11 (2009) 262–265.
[20] H.B. Wang, Q.M. Pan, J.W. Zhao, G.P. Yin, P.J. Zuo, J. Power Sources 167 (2007) 206–211.
[21] X.H. Huang, J.P. Tu, Y.Z. Yang, J.Y. Xiang, Electrochem. Commun. 10 (2008) 16–19.
[22] H.C. Liu, S.K. Yen, J. Power Sources 166 (2007) 478–484.
[23] S.-L. Chou, J.-Z. Wang, H.-K. Liu, S.-X. Dou, J. Power Sources 182 (2008) 359–364.